iScience

CellPress
OPEN ACCESS

Article

A pair of commissural command neurons induces *Drosophila* wing grooming

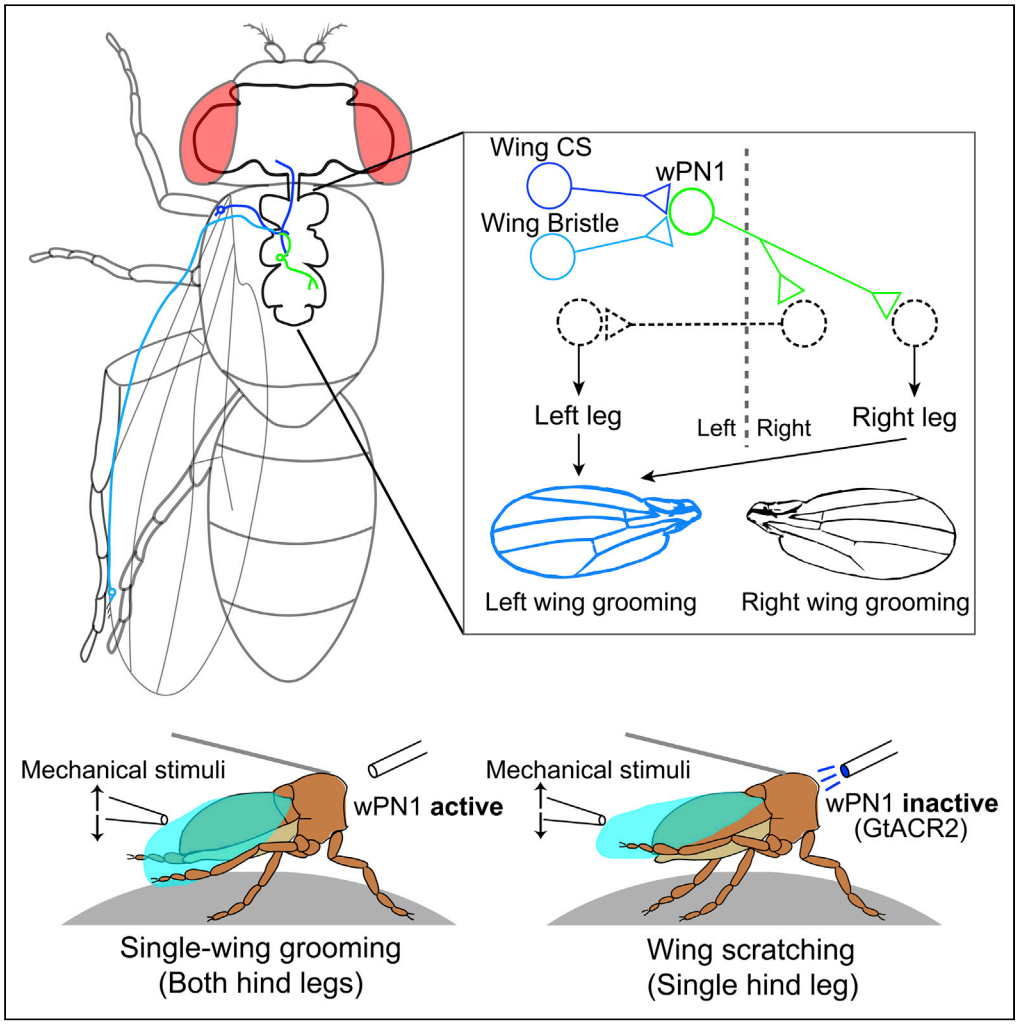

Neil Zhang, Julie H. Simpson

jhsimpson@ucsb.edu

Highlights

A pair of ventral cord neurons, wPN1, is sufficient and necessary for wing grooming

wPN1 receive contacts from two types of wing mechanosensors

wPN1 are cholinergic and have commissural projections

Single-side activation of wPN1 drives both hind legs to clean the ipsilateral wing

Zhang & Simpson, iScience 25, 103792
February 18, 2022
https://doi.org/10.1016/j.isci.2022.103792

iScience

CellPress
OPEN ACCESS

Article

A pair of commissural command neurons induces *Drosophila* wing grooming

Neil Zhang[1] and Julie H. Simpson[1,2,*]

SUMMARY

In many behaviors such walking and swimming, animals need to coordinate their left and right limbs. In *Drosophila*, wing grooming can be induced by activation of sensory organs called campaniform sensilla. Flies usually clean one wing at a time, coordinating their left and right hind legs to sweep the dorsal and ventral surfaces of the wing. Here, we identify a pair of interneurons located in the ventral nerve cord that we name wing projection neurons 1 (wPN1) whose optogenetic activation induces wing grooming. Inhibition of wPN1 activity reduces wing grooming. They receive synaptic input from ipsilateral wing campaniform sensilla and wing mechanosensory bristle neurons, and they extend axonal arbors to the hind leg neuropils. Although they project contralaterally, their activation induces ipsilateral wing grooming. Anatomical and behavioral data support a role for wPN1 as command neurons coordinating both hind legs to work together to clean the stimulated wing.

INTRODUCTION

The central nervous system integrates the sensory information it receives and coordinates motor neurons controlling the limbs to accomplish the movements we observe as behavior, but the essential neural circuits are still largely unknown. We use fly grooming as a model to investigate this process. When covered with dust, fruit flies follow an anterior-to-posterior sequence to clean their bodies (Mueller et al., 2022; Seeds et al., 2014). In anterior grooming, flies coordinate front legs to clean the head and then discard dust through front leg rubbing. In posterior grooming, flies clean the abdomen and wings with their hind legs and then rub them together to remove accumulated dust. Our previous study shows that this grooming sequence is induced by spatial comparisons of mechanosensory information (Zhang et al., 2020). In order to identify the neural circuits that govern the choice between anterior and posterior grooming, we first need to elucidate the interneurons organizing each grooming subroutine. Using a combination of anatomically guided selection of genetic reagents and behavioral screening, we previously mapped neural circuitry controlling antennal grooming (Hampel et al., 2015). Here, we employ a similar approach to investigate components that contribute to wing grooming.

RESULTS

Wing grooming can be induced by wing campaniform sensilla in both intact and decapitated flies

Grooming can be induced by several types of mechanosensory neurons including campaniform sensilla (Hampel et al., 2017; Zhang et al., 2020). In a previous screen (Zhang et al., 2020), we identified the *Wing haltere CS-spGAL4* driver line, which labels campaniform sensilla on both wings and halteres. Approximately 80 wing campaniform sensilla are found on a single wing, and they can be classified as proximal or distal according to their location relative to the wing hinge (Cole and Palka, 1982; Dinges et al., 2021). Our driver line consistently labels approximately 20 proximal sensilla with projections into the ventral nerve cord (VNC) and the subesophageal zone of the brain (Figures 1A–1C) (Ghysen, 1980).

Optogenetic activation of these wing campaniform sensilla (*Wing haltere CS-spGAL4> CsChrimson*) induced strong wing grooming (Figures 1E, S1D and S1E). The same response was still observed upon haltere removal (data not shown), which suggests that wing campaniform sensilla play the essential role. This driver line also labels ~14 interneurons near the optic lobe, but wing grooming was still induced in decapitated flies (Figures 1E and S1E), indicating these brain neurons are not required. The response in decapitated flies also suggests that neural circuits within VNC are sufficient for wing grooming.

[1]Department of Molecular, Cellular and Developmental Biology and Neuroscience Research Institute, University of California, Santa Barbara, CA 93106, USA

[2]Lead contact

*Correspondence: jhsimpson@ucsb.edu

https://doi.org/10.1016/j.isci.2022.103792

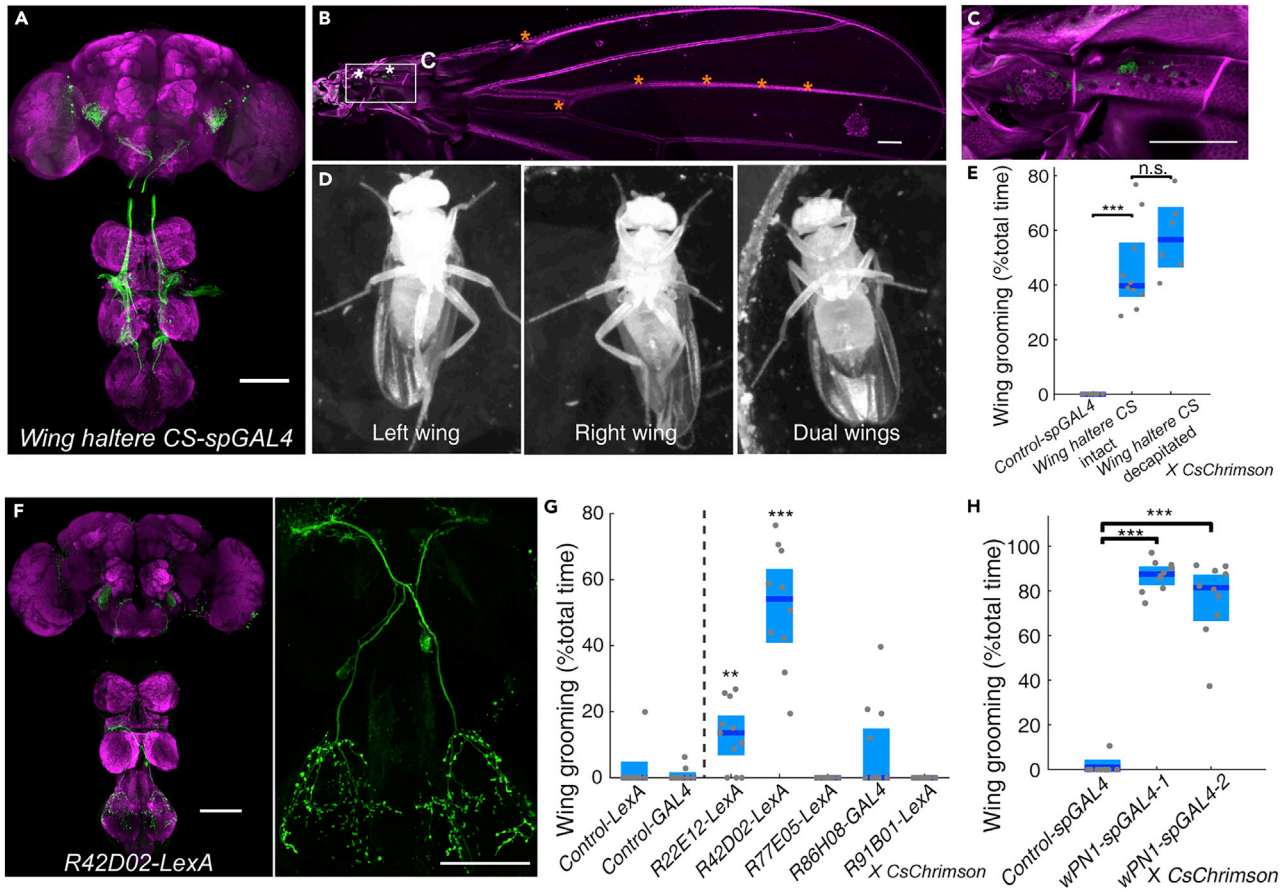

Figure 1. Identification of wPN1, a pair of projection neurons that induce wing grooming upon optogenetic activation

(A–C) Expression pattern of *Wing haltere CS-spGAL4* in the central nervous system (CNS) (A) and wing (B, C). Green, anti-GFP. Magenta, anti-Bruchpilot in CNS, cuticle autofluorescence in wing. Proximal campaniform sensilla are indicated by white asterisks; distal campaniform sensilla are indicated by orange asterisks in (B) Scale bars, 100 μm.

(D) Video screenshots showing subtypes of wing grooming. Videos were recorded from below.

(E) Quantification of wing grooming during light activation.

(F) Expression pattern of *R42D02-lexA* in CNS.

(G) Percent time flies spend in wing grooming during 1-min photoactivation of candidate wing campaniform sensilla downstream neurons.

(H) Percent time flies spend in wing grooming during 1-min photoactivation of wPN1 targeted by *wPN1-spGAL4-1* and *wPN1-spGAL4-2*. Each gray point represents a single fly. The 95% confidence intervals for the mean are shown as light blue shades. The median is shown as a blue line. Kruskal-Wallis test and Wilcoxon rank-sum post hoc with Bonferroni correction were used for significant test. *p < 0.05; **p < 0.01; ***p < 0.001.

Dust-covered flies can clean both wings at once, but usually they clean one wing at a time, using both hind legs in a coordinated manner to sweep the dorsal and ventral surfaces of the same wing. We refer to this as single-wing grooming. Optogenetic activation of campaniform sensilla in undusted flies induces both types of wing grooming, and single-wing grooming is also more common, employing both left and right hind legs (Figures 1D and S1F). Dust-induced and optogenetically induced wing grooming look similar to human observers, and both can be reliably recognized by our automatic behavior recognition system (ABRS) (Ravbar et al., 2019). With bilateral activation of wing campaniform sensilla, flies spend approximately equal amounts of time performing single-wing grooming of the left or right wing (Figure S1F).

Identification of wPN1, a pair of projection neurons that induce wing grooming upon optogenetic activation

To identify secondary interneurons receiving inputs from wing campaniform sensilla, we used *trans*-Tango, a tool for anterograde tracing (Talay et al., 2017). We expressed the *trans*-Tango ligand in wing campaniform sensilla and its membrane-targeted receptors using a broad neuronal driver to identify post-synaptic candidates (indicated by mtdTomato-HA reporter expression). Using the anatomy of these Tango-positive

neurons as a template (Figure S1G), we searched through the literature and Fly Light expression pattern data (Jenett et al., 2012; Robie et al., 2017) for driver lines that target these candidate interneurons.

Five sparse driver lines were identified by anatomical criteria and then tested in an activation screen. We found that the *R42D02-LexA* driver line can induce strong wing grooming upon optogenetic activation (Figure 1G). *R42D02-LexA* labels one pair of intersegmental interneurons with neurites in the wing neuropil and T3 (Figure 1F). We name these "wing projection neurons 1" (wPN1) since they may connect wing sensory inputs to hind leg motor circuits. We generated two additional split-GAL4 combinations that also target wPN1 (Figures S1H and S1I). All three lines exclusively induce wing grooming during optogenetic activation (Figures 1G, 1H and S1J–S1L).

wPN1 are necessary for wing grooming

Dust induces grooming behavior in *Drosophila*, and grooming contains sequential subroutines including front leg rubbing, head cleaning, abdominal cleaning, back leg rubbing, and wing grooming. Wing grooming usually happens late in the grooming sequence.

To investigate the role of wPN1 in dust-induced grooming behavior, we used the blue light-sensitive chloride channel GtACR2 to inhibit their activity (Mohammad et al., 2017). Using our standard grooming assay for freely moving, dust-covered flies, we find that silencing wPN1 strongly reduces wing grooming. Control flies remove dust from their wings within 22 min, whereas the *wPN1-spGAL4-1>GtACR2* flies' wings remain dirty (Figure 2A). The observation of reduced wing grooming based on residual dust is supported by behavior quantification using ABRS: inhibition of wPN1 through GtACR2 almost completely eliminates dust-induced wing grooming movements (Figure 2B). We confirmed this phenotype with an alternative neuronal silencer by expressing an inward-rectifying potassium channel, Kir2.1, in wPN1 (Figures S2A–S2D).

To look at the leg movements during wing grooming in more detail, we tested the effects of wPN1 inhibition in a tethered "fly-on-a-ball" setup (Figure 2C) (Seelig et al., 2010). Since precise local application of dust to the wings is challenging, and damaging to the instruments, we chose defined mechanical stimulation instead. Decapitated flies will respond to a small mechanical deflection of the wings with one of three behaviors: wing "scratching," single-wing grooming, or a dual-wing sweep. During wing scratching, flies use one hind leg to scratch one surface of a single wing. During single-wing grooming, flies use both hind legs to clean both surfaces of a single wing (Figure 2D). In the dual-wing sweep, flies use both hind legs in parallel, with the left leg sweeping the left wing and the right leg sweeping the right wing. Single-wing grooming is the most common response, whereas dual-wing sweep is rare.

In our experiments, 90 s of mechanical stimulation is applied to tethered flies at 2 Hz using a pipet tip mounted on a micromanipulator. 30 s of blue light is also presented in the middle to activate GtACR2, silencing wPN1. We used decapitated flies to avoid the startle response to blue light (Figure 2C). The light did not change the time control flies spend on the three types of wing grooming behaviors, but in experimental flies where wPN1 is inhibited by GtACR2, single-wing grooming was specifically reduced. Wing scratching was not affected (Figures 2E and S2E). Therefore, our experiment suggests that wPN1 are necessary for single-wing grooming, where both hind legs cooperate, whereas wing scratching can be accomplished by other circuits.

Together with the activation data, our loss-of-function experiments make wPN1 candidate command neurons for wing grooming (Kupfermann and Weiss, 1978).

wPN1 are cholinergic and receive direct sensory inputs from wing mechanosensory neurons

The neurites of wPN1 show different morphology: branches near the wing neuropil are smooth, whereas the ones in T3 are varicose, harboring structures similar to synaptic boutons (Figures 1F, S1H and S1I). To confirm the polarity of wPN1, we expressed the dendritic reporter DenMark and the presynaptic reporter syt-GFP (Nicolaï et al., 2010). The result indicates that wPN1 has dendrites in wing neuropil, whereas its presynaptic sites are mainly located in the T3 region of the VNC (Figure 3A).

The structure and location of wPN1 suggests they may receive direct inputs from wing sensory neurons. Double-labeling experiments show that projections from wing campaniform sensilla and wPN1 are very close to each other in wing neuropil (Figure 3C). We also tested potential contact using GRASP, "genetic

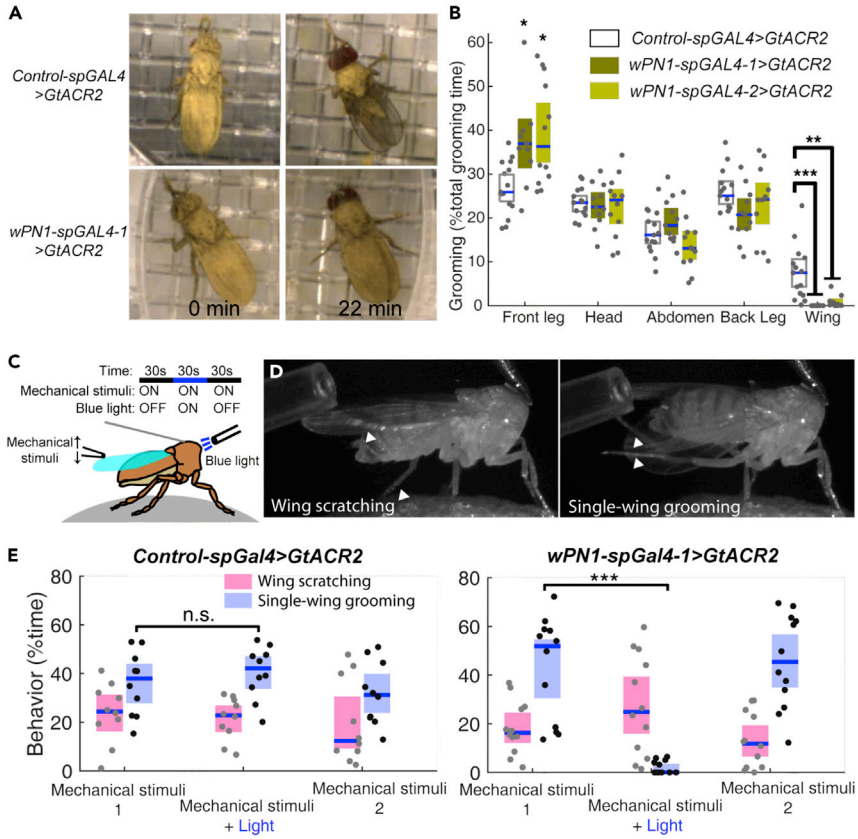

Figure 2. wPN1 inhibition disrupts wing grooming

(A) Video screenshots showing the dust distribution in a control fly and a fly with wPN1 inhibition at different time points.

(B) Percent of time each behavior performed by dusted flies with wPN1 inhibition and dusted control flies. Wing grooming is significantly reduced in flies with wPN1 inhibition.

(C) Schematic of "fly-on-a-ball" system. A light fiber delivers blue light to the thorax of a decapitated fly. A pipette tip attached to a micromanipulator performs mechanical stimuli to the wings at ~2 Hz. Each 90-s experiment was separated into three episodes. Mechanical stimuli were delivered throughout the whole experiment. Constant blue light was only turned on during the middle 30 s.

(D) Video screenshots showing wing scratching (performed by one leg) and single wing grooming (performed by both hind legs).

(E) Quantification of different wing cleaning behaviors induced by mechanical stimuli with and without wPN1 inhibition. Individual data points, median line, and 95% confidence intervals for the mean are shown in the figures. Kruskal-Wallis test and Wilcoxon rank-sum post hoc with Bonferroni correction were used for comparisons in (B). Wilcoxon signed-rank test was used for comparisons in (E). *$p < 0.05$; **$p < 0.01$; ***$p < 0.001$.

reconstitution of GFP between synaptic partners" (Feinberg et al., 2008). Here, one fragment of GFP was expressed using *Wing haltere CS-spGAL4*, and the complementary fragment using *R42D02-LexA*. Strong reconstituted GFP signal was observed in wing neuropil in experimental flies but not in controls (Figure 3D).

Besides campaniform sensilla, wing bristles can also induce wing grooming. Both double-labeling and GRASP experiments indicate that wPN1 also form synaptic connections with bristle neurons (Figures 3E and 3F). The bristle driver lines we use label extra bristles on other body parts, so further experiments were performed to confirm the specificity of the GRASP signals. First, we used synaptic GRASP (Macpherson et al., 2015) where one fragment GFP is expressed specifically in the axons of presynaptic neurons. Reconstituted GFP signal was still observed in experimental flies but not in controls (Figures S4B and S4C). Second, the right wing was removed to induce the degradation of wing bristle neurons. As a result, the GRASP signals on the right side were greatly reduced, confirming that the bristle neurons connecting to wPN1 originate in the wing (Figure S4D). Since neural activity from either type of mechanosensory neuron

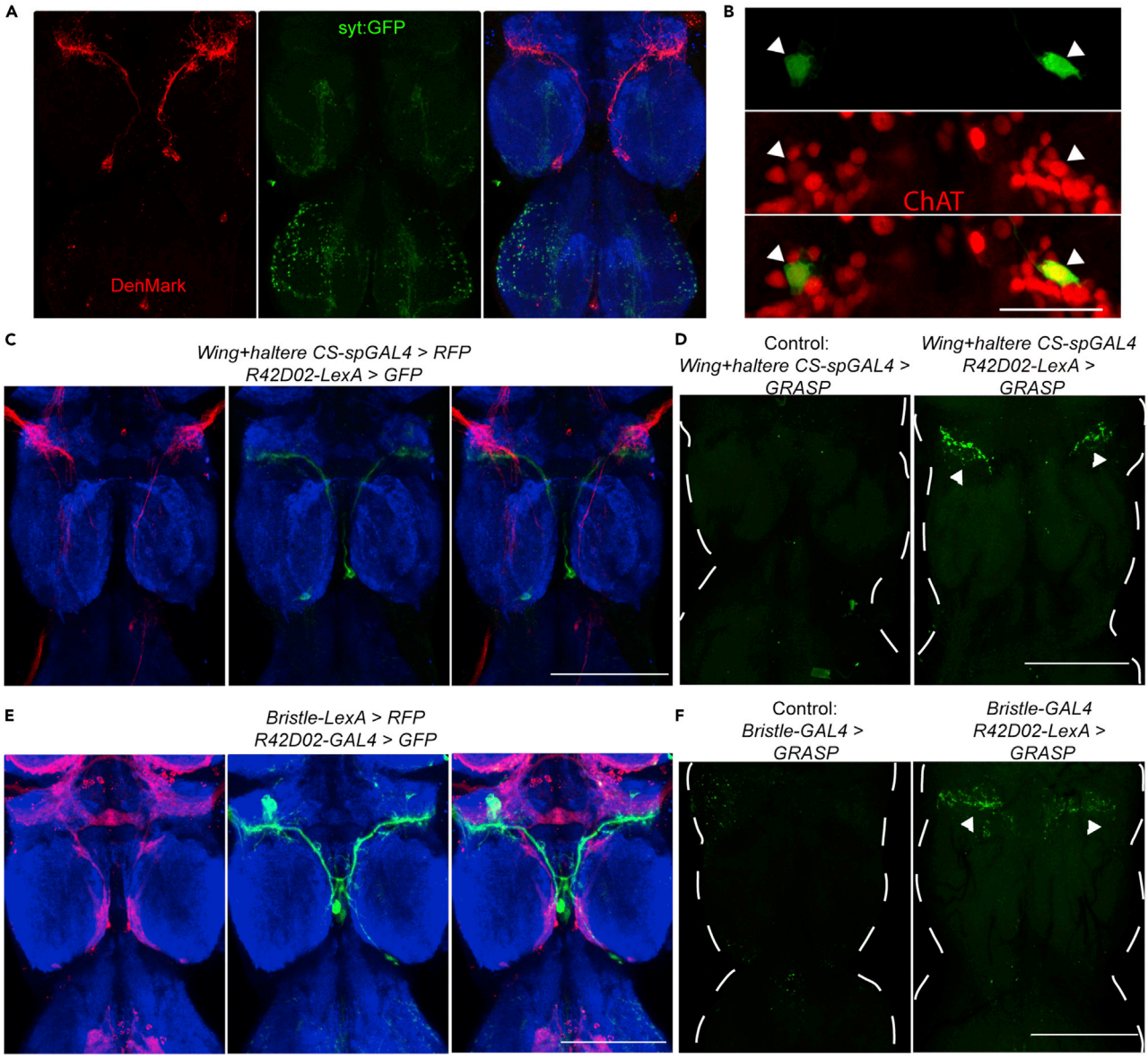

Figure 3. wPN1 receive direct sensory inputs from wing mechanosensory neurons and send excitatory outputs near the hind leg motor circuits

(A) Expression pattern of dendritic marker (Denmark, red) and axonal marker (syt-GFP, green) driven by *wPN1-spGAL4-2* in VNC. Green, anti-GFP. Red, anti-RFP. Blue, anti-Bruchpilot.

(B) Double labeling of wPN1 (*R42D02-GAL4*, green) with cholinergic neurons (*ChAT-LexA*, red). White arrowheads indicate the position of the wPN1 cell bodies. Scale bars, 25 μm.

(C) Co-labeling of wCS neurons (red) and wPN1 (green) in VNC. Scale bars, 100 μm.

(D) GRASP reconstituted GFP signal (green) between wing campaniform sensilla neurons and wPN1 in the wing neuropil (right). White arrowheads indicate wPN1 dendrites. GRASP signal was not observed in control flies (left).

(E) Co-labeling of bristle neurons (red) and wPN1 (green) in VNC. Scale bars, 100 μm.

(F) GRASP reconstituted GFP signal between bristle neurons and wPN1 in the wing neuropil (right; white arrowheads). GRASP signal was not observed in control flies (left).

is sufficient to induce wing grooming, the connectivity suggests that wPN1 may integrate sensory information from both wing campaniform sensilla and bristles.

Next, we investigated the neurotransmitter identity of wPN1. Acetylcholine, GABA, and glutamate are the main fast-acting neurotransmitters in *Drosophila*. Acetylcholine is excitatory, GABA is inhibitory, and

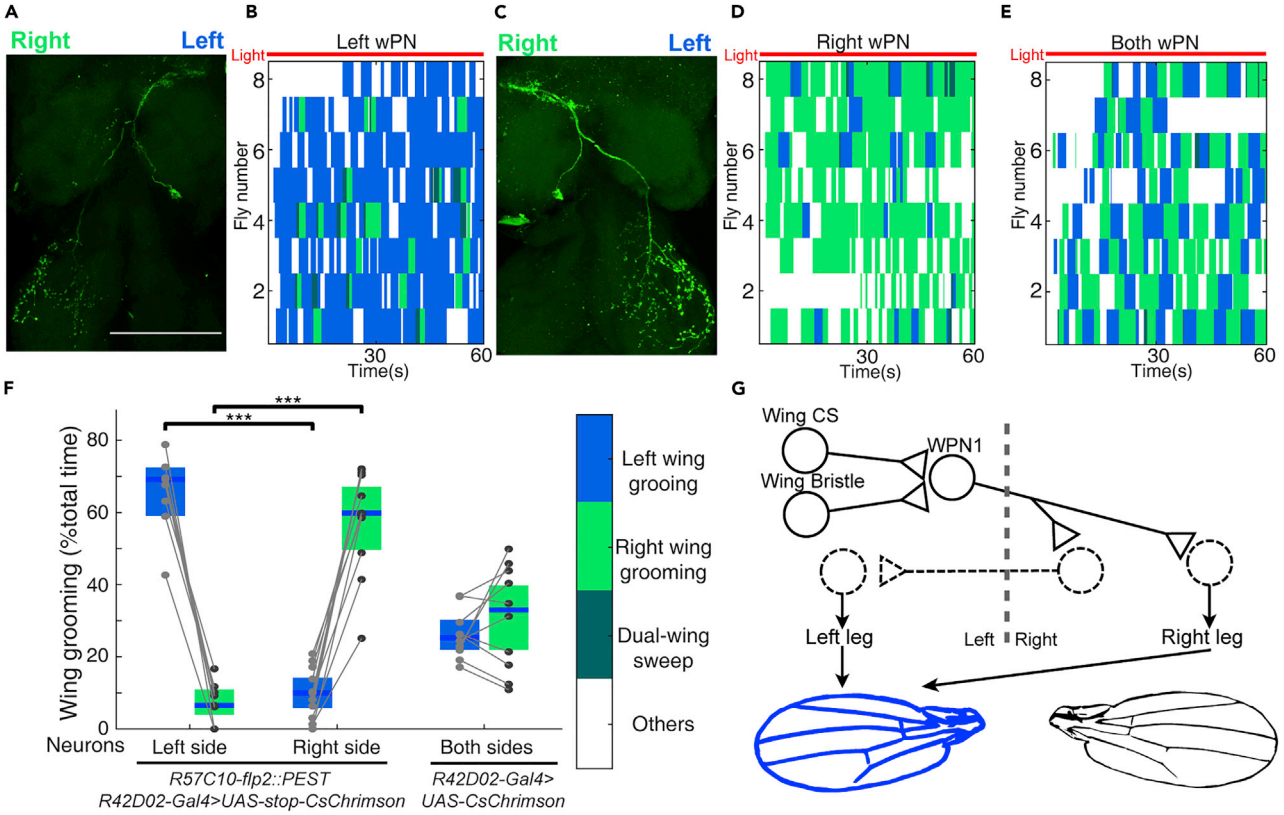

Figure 4. wPN1 have contralateral projections but induce wing grooming ipsilaterally

(A and C) Stochastically labeled single wPN1 interneuron on the left (A) or the right side (C). The left-right axis is reversed because of the sample direction. Scale bars, 100 μm.

(B, D and E) Different types of wing grooming induced by optogenetic activation of the left side (B), right side (D), or both sides (E) of wPN1.

(F) Quantification of different wing grooming subtypes induced by one side or both sides of wPN1.

(G) Schematic of the wPN1 circuit for wing grooming where known components are represented with solid outlines and proposed elements are dashed. Left wPN1 receives information from campaniform sensilla and mechanosensory bristles on the left wing. It then transfers signals across the midline and initiates movements of the right leg. At the same time, a group of commissural neurons sends outputs to the left leg. Both hind legs work together to groom the left wing. Individual data points, median line, and 95% confidence intervals for the mean are shown in the figures. Wilcoxon rank-sum test was used for significant test. *p < 0.05; **p < 0.01; ***p < 0.001.

glutamate can be either depending on the post-synaptic receptor (Lacin et al., 2019). wPN1 are only labeled by the acetylcholine marker *Chat-LexA* (Figures 3B, S3B and S3C). Several lines of behavioral and immunohistochemical evidence further demonstrate that wPN1 are cholinergic excitatory neurons (Figures S3D–S3J). Both wing campaniform sensilla and bristle neurons are also labeled by *Chat-LexA*, indicating that they too are cholinergic (Figure S3A), as expected. These data indicate that wPN1 receive direct synaptic inputs from wing mechanosensory neurons and send excitatory outputs near the hind leg motor circuits.

wPN1 transfer sensory information across the midline

Activation of both wPN1 induces wing grooming, just like activation of the wing campaniform sensilla: flies clean one wing at a time, using both hind legs together, and switch back and forth between left and right wings (Figures 4E and 4F). To investigate how the grooming of each side is controlled, we performed stochastic activation of wPN1 on only one side.

We expressed *UAS-FRT > -STOP-FRT > -CsChrimson* in wPN1 using *R42D02-GAL4*. At the same time, the R57C10 promoter drives the expression of *Flp2::PEST* in all neurons; the PEST sequence reduces the half-life of Flp2 recombinase (Li et al., 1998), generating sparse clones of CsChrimson expression within the *R42D02-GAL4* pattern. Each individual fly was tested by 1-min optogenetic activation and then dissected

for central nervous system imaging. We analyzed flies in which only a single wPN1 is targeted. Surprisingly, although a wPN1 receives sensory input from one side and projects axons to the other side of the body (Figures 4A and 4C), wing grooming was mainly induced on the same side as the sensory input (Figures 4B, 4D and 4F). Therefore, wPN1 receive inputs from wing mechanosensory neurons and project contralaterally, but induce wing grooming ipsilaterally, recruiting participation of both hind legs.

Interneurons with commissural projections are found in both invertebrates and vertebrates, where they compare sensory inputs or coordinate motor outputs (Gebhardt and Honegger, 2001; Heckscher et al., 2015; Lai et al., 2012; Lanuza et al., 2004; Linneweber et al., 2020; Suster et al., 2009; Suver et al., 2019; Talpalar et al., 2013; Tuthill and Wilson, 2016). In *Drosophila*, they have been identified in auditory (Lai et al., 2012), visual (Linneweber et al., 2020), and mechanosensory (Suver et al., 2019; Tuthill and Wilson, 2016) neural circuits, where they transmit sensory information across the midline. Excitatory contralateral interneurons are also found in larva, where they contribute to symmetric bilateral muscle contraction (Heckscher et al., 2015).

During single-wing grooming, flies use both hind legs to clean a single wing. Therefore, sensory information from one wing is expected to cross the midline and activate motor output on the other side. The morphology of wPN1 suggests that they may play an essential role in this process. For example, left wPN1 transmits information from the left wing contralaterally, driving the right leg to clean the left wing (Figure 4G). The left wPN1 may indirectly induce movements of the left leg as well, through downstream commissural neurons, as wPN1 axons overlap with several commissures in the adult *Drosophila* VNC T3, including the ventral anterior intermediate commissure and posterior intermediate commissure (Figure S4E) (Court et al., 2020). This circuit configuration can also explain the phenotype we observed in the fly-on-the-ball experiment: when wPN1 are inhibited, the command signal to the contralateral leg is interrupted and the fly cannot use both hind legs to clean a single wing (Figures 2E and S2E).

wPN1 do not connect directly to motor neurons

Last, we investigated the neurons downstream of wPN1. Although our wPN1 *trans*-Tango experiments were inconclusive (data not shown), we detected direct GRASP contact between wPN1 and cholinergic neurons but not GABAergic or glutamatergic ones (Figures S4F–S4I). Since glutamate is the main neurotransmitter of *Drosophila* motor neurons (Johansen et al., 1989), these results suggest that motor neurons are not direct partners of wPN1. The circuits downstream of wPN1 that bridge the midline and the pre-motor neurons that achieve the coordinated movements of left and right legs for wing grooming are the subject of ongoing neuronal tracing studies using new connectomic resources (Phelps et al., 2021).

DISCUSSION

We have identified wPN1 as potential command neurons for wing grooming. Although the criteria for command neurons is debated (Kupfermann and Weiss, 1978; Yoshihara and Yoshihara, 2018), neurons whose activation can induce a coherent motor program and whose function is required for that behavior to occur normally, such as wPN1, provide important entry points to map the neural circuits governing that behavior.

Our characterization of wPN1 reveals additional complexities in the control of grooming. Wing scratch remains unaffected, indicating additional sensory-to-motor pathways between wings and legs. Other left-right coordination circuits must also exist, since inhibition of wPN1 disrupts wing grooming but leaves hind-leg rubbing largely normal. wPN1 provides an entry point to identify downstream commissural and pre-motor neurons that coordinate left and right leg movements.

Wing cleaning normally occurs late in the hierarchical sequence of grooming subroutines, and wPN1 may provide insights into when it is selected. Perhaps sensory information from wing campaniform sensilla and mechanosensory bristles integrate or accumulate to a threshold sufficient to activate wPN1, or perhaps wPN1 is transiently inhibited by circuits driving other grooming behaviors. Identification of wPN1 makes these testable hypotheses with the potential to reveal a general control mechanism for sequential motor behaviors.

Limitations of the study

Our behavior and anatomy data provide strong evidence that wPN1 plays an essential, command-like role in coordinating left and right back legs, but higher-resolution behavioral analysis and complete neuronal circuit mapping downstream of wPN1 are necessary to confirm.

STAR★METHODS

Detailed methods are provided in the online version of this paper and include the following:

- KEY RESOURCES TABLE
- RESOURCE AVAILABILITY
  - Lead contact
  - Materials availability
  - Data and code availability
- EXPERIMENTAL MODEL AND SUBJECT DETAILS
- METHOD DETAILS
  - Immunofluorescence and confocal imaging
  - Optogenetic activation experiments of free-moving flies
  - Recording and analysis of dust-induced grooming with optogenetic inhibition
  - Fly-on-a-ball experiment
- QUANTIFICATION AND STATISTICAL ANALYSIS

SUPPLEMENTAL INFORMATION

Supplemental information can be found online at https://doi.org/10.1016/j.isci.2022.103792.

ACKNOWLEDGMENTS

We thank Barry J. Dickson, Andrew M. Seeds, and Stefanie Hampel for fly strains and Simpson, Louis, and Kim lab members for input on the manuscript. We thank HHMI, UCSB, and NIH R01NS110866 for funding.

AUTHOR CONTRIBUTIONS

Conceptualization, N.Z. and J.H.S.; investigation, N.Z.; writing, N.Z. and J.H.S.; funding acquisition, J.H.S.; supervision, J.H.S.

DECLARATION OF INTERESTS

The authors declare no competing interests.

Received: April 29, 2021
Revised: January 3, 2022
Accepted: January 13, 2022
Published: February 18, 2022

REFERENCES

Cole, E.S., and Palka, J. (1982). The pattern of campaniform sensilla on the wing and haltere of Drosophila melanogaster and several of its homeotic mutants. Development *71*, 41–61.

Court, R., Namiki, S., Armstrong, J.D., Börner, J., Card, G., Costa, M., Dickinson, M., Duch, C., Korff, W., and Mann, R. (2020). A systematic nomenclature for the Drosophila ventral nerve cord. Neuron *107*, 1071–1079.

Dinges, G.F., Chockley, A.S., Bockemühl, T., Ito, K., Blanke, A., and Büschges, A. (2021). Location and arrangement of campaniform sensilla in Drosophila melanogaster. J. Comp. Neurol. *529*, 905–925.

Feinberg, E.H., VanHoven, M.K., Bendesky, A., Wang, G., Fetter, R.D., Shen, K., and Bargmann, C.I. (2008). GFP reconstitution across synaptic partners (GRASP) defines cell contacts and synapses in living nervous systems. Neuron *57*, 353–363.

Gebhardt, M., and Honegger, H.-W. (2001). Physiological characterisation of antennal mechanosensory descending interneurons in an insect (Gryllus bimaculatus, Gryllus campestris) brain. J. Exp. Biol. *204*, 2265–2275.

Ghysen, A. (1980). The projection of sensory neurons in the central nervous system of Drosophila: choice of the appropriate pathway. Developmental Biol. *78*, 521–541.

Gordon, M.D., and Scott, K. (2009). Motor control in a Drosophila taste circuit. Neuron *61*, 373–384.

Hampel, S., Franconville, R., Simpson, J.H., and Seeds, A.M. (2015). A neural command circuit for grooming movement control. eLife *4*. https://doi.org/10.7554/eLife.08758.

Hampel, S., McKellar, C.E., Simpson, J.H., and Seeds, A.M. (2017). Simultaneous activation of parallel sensory pathways promotes a grooming sequence in drosophila. eLife *6*. https://doi.org/10.7554/eLife.28804.

Heckscher, E.S., Zarin, A.A., Faumont, S., Clark, M.Q., Manning, L., Fushiki, A., Schneider-Mizell, C.M., Fetter, R.D., Truman, J.W., and Zwart, M.F. (2015). Even-skipped+ interneurons are core components of a sensorimotor circuit that maintains left-right symmetric muscle contraction amplitude. Neuron *88*, 314–329.

Jenett, A., Rubin, G.M., Ngo, T.-T.B., Shepherd, D., Murphy, C., Dionne, H., Pfeiffer, B.D., Cavallaro, A., Hall, D., Jeter, J., et al. (2012). A GAL4-driver line resource for Drosophila neurobiology. Cell Rep. *2*, 991–1001. https://doi.org/10.1016/j.celrep.2012.09.011.

Johansen, J., Halpern, M.E., Johansen, K.M., and Keshishian, H. (1989). Stereotypic morphology of glutamatergic synapses on identified muscle cells of Drosophila larvae. J. Neurosci. *9*, 710–725.

Kupfermann, I., and Weiss, K.R. (1978). The command neuron concept. Behav. Brain Sci. *1*, 3–10.

Lacin, H., Chen, H.-M., Long, X., Singer, R.H., Lee, T., and Truman, J.W. (2019). Neurotransmitter identity is acquired in a lineage-restricted manner in the Drosophila CNS. Elife *8*, e43701.

Lai, J.S.-Y., Lo, S.-J., Dickson, B.J., and Chiang, A.-S. (2012). Auditory circuit in the Drosophila brain. Proc. Natl. Acad. Sci. U S A *109*, 2607–2612.

Lanuza, G.M., Gosgnach, S., Pierani, A., Jessell, T.M., and Goulding, M. (2004). Genetic identification of spinal interneurons that coordinate left-right locomotor activity necessary for walking movements. Neuron *42*, 375–386.

Li, X., Zhao, X., Fang, Y., Jiang, X., Duong, T., Fan, C., Huang, C.-C., and Kain, S.R. (1998). Generation of destabilized green fluorescent protein as a transcription reporter. J. Biol. Chem. *273*, 34970–34975.

Linneweber, G.A., Andriatsilavo, M., Dutta, S.B., Bengochea, M., Hellbruegge, L., Liu, G., Ejsmont, R.K., Straw, A.D., Wernet, M., and Hiesinger, P.R. (2020). A neurodevelopmental origin of behavioral individuality in the Drosophila visual system. Science *367*, 1112–1119.

Macpherson, L.J., Zaharieva, E.E., Kearney, P.J., Alpert, M.H., Lin, T.-Y., Turan, Z., Lee, C.-H., and Gallio, M. (2015). Dynamic labelling of neural connections in multiple colours by trans-synaptic fluorescence complementation. Nat. Commun. *6*, 1–9.

Mohammad, F., Stewart, J.C., Ott, S., Chlebikova, K., Chua, J.Y., Koh, T.W., Ho, J., and Claridge-Chang, A. (2017). Optogenetic inhibition of behavior with anion channelrhodopsins. Nat. Methods *14*, 271–274. https://doi.org/10.1038/nmeth.4148.

Mueller, J.M., Zhang, N., Carlson, J.M., and Simpson, J.H. (2022). Variation and variability in Drosophila grooming behavior. Front. Behav. Neurosci. *15*. https://doi.org/10.3389/fnbeh.2021.769372.

Nern, A., Pfeiffer, B.D., and Rubin, G.M. (2015). Optimized tools for multicolor stochastic labeling reveal diverse stereotyped cell arrangements in the fly visual system. Proc. Natl. Acad. Sci. U S A *112*, E2967–E2976.

Nicolaï, L.J.J., Ramaekers, A., Raemaekers, T., Drozdzecki, A., Mauss, A.S., Yan, J., Landgraf, M., Annaert, W., and Hassan, B.A. (2010). Genetically encoded dendritic marker sheds light on neuronal connectivity in Drosophila. Proc. Natl. Acad. Sci. U S A *107*, 20553–20558.

Phelps, J.S., Hildebrand, D.G.C., Graham, B.J., Kuan, A.T., Thomas, L.A., Nguyen, T.M., Buhmann, J., Azevedo, A.W., Sustar, A., and Agrawal, S. (2021). Reconstruction of motor control circuits in adult Drosophila using automated transmission electron microscopy. Cell *184*, 759–774.

Ravbar, P., Branson, K., and Simpson, J.H. (2019). An automatic behavior recognition system classifies animal behaviors using movements and their temporal context. J. Neurosci. Methods *326*, 108352. https://doi.org/10.1016/j.jneumeth.2019.108352.

Robie, A.A., Hirokawa, J., Edwards, A.W., Umayam, L.A., Lee, A., Phillips, M.L., Card, G.M., Korff, W., Rubin, G.M., and Simpson, J.H. (2017). Mapping the neural substrates of behavior. Cell *170*, 393–406.

Seeds, A.M., Ravbar, P., Chung, P., Hampel, S., Midgley, F.M., Mensh, B.D., and Simpson, J.H. (2014). A suppression hierarchy among competing motor programs drives sequential grooming in Drosophila. eLife *3*, e02951. https://doi.org/10.7554/eLife.02951.

Seelig, J.D., Chiappe, M.E., Lott, G.K., Dutta, A., Osborne, J.E., Reiser, M.B., and Jayaraman, V. (2010). Two-photon calcium imaging from head-fixed Drosophila during optomotor walking behavior. Nat. Methods *7*, 535–540. https://doi.org/10.1038/nmeth.1468.

Shirangi, T.R., Wong, A.M., Truman, J.W., and Stern, D.L. (2016). Doublesex regulates the connectivity of a neural circuit controlling Drosophila male courtship song. Developmental Cel. *37*, 533–544.

Suster, M.L., Kania, A., Liao, M., Asakawa, K., Charron, F., Kawakami, K., and Drapeau, P. (2009). A novel conserved evx1 enhancer links spinal interneuron morphology and cis-regulation from fish to mammals. Developmental Biol. *325*, 422–433.

Suver, M.P., Matheson, A.M.M., Sarkar, S., Damiata, M., Schoppik, D., and Nagel, K.I. (2019). Encoding of wind direction by central neurons in Drosophila. Neuron *102*, 828–842.e7. https://doi.org/10.1016/j.neuron.2019.03.012.

Talay, M., Richman, E.B., Snell, N.J., Hartmann, G.G., Fisher, J.D., Sorkaç, A., Santoyo, J.F., Chou-Freed, C., Nair, N., and Johnson, M. (2017). Transsynaptic mapping of second-order taste neurons in flies by trans-Tango. Neuron *96*, 783–795.

Talpalar, A.E., Bouvier, J., Borgius, L., Fortin, G., Pierani, A., and Kiehn, O. (2013). Dual-mode operation of neuronal networks involved in left–right alternation. Nature *500*, 85–88.

Tuthill, J.C., and Wilson, R.I. (2016). Parallel transformation of tactile signals in central circuits of Drosophila. Cell *164*, 1046–1059. https://doi.org/10.1016/j.cell.2016.01.014.

von Reyn, C.R., Breads, P., Peek, M.Y., Zheng, G.Z., Williamson, W.R., Yee, A.L., Leonardo, A., and Card, G.M. (2014). A spike-timing mechanism for action selection. Nat. Neurosci. *17*, 962–970. https://doi.org/10.1038/nn.3741.

Yoshihara, M., and Yoshihara, M. (2018). 'Necessary and sufficient'in biology is not necessarily necessary–confusions and erroneous conclusions resulting from misapplied logic in the field of biology, especially neuroscience. J. Neurogenet. *32*, 53–64.

Zhang, N., Guo, L., and Simpson, J.H. (2020). Spatial comparisons of mechanosensory information govern the grooming sequence in Drosophila. Curr. Biol. CB *30*, 988–1001.e4. https://doi.org/10.1016/j.cub.2020.01.045.

STAR★METHODS

KEY RESOURCES TABLE

REAGENT or RESOURCE	SOURCE	IDENTIFIER
Antibodies		
chicken polyclonal to GFP	Abcam	Cat#13970
rabbit polyclonal to GFP	Invitrogen	Cat#A-11122
rabbit monoclonal anti-HA	Cell Signaling Technologies	Cat# C29F4
mouse monoclonal brp antibody	DSHB	Cat#AB_2314866
anti-chicken Alexa Fluor 488	Invitrogen	Cat#A-11039
anti-rabbit Alexa Fluor 488	Invitrogen	Cat#A-11008
anti-rabbit Alexa Fluor 568	Invitrogen	Cat# A-11011
anti-mouse Alexa Fluor 633	Invitrogen	Cat#A-21052
Chemicals, peptides, and recombinant proteins		
Reactive Yellow 86	Organic Dyestuffs Corporation	CAS 61951-86-8
Insect-a-slip	BioQuip Products	Cat#2871A
UV glue	Bondic	N/A
Deposited data		
Ethogram data	This paper; Mendeley Data	https://doi.org/10.17632/87ngcrv7xw.1
Experimental models: Organisms/strains		
Canton S	Bloomington Stock Center	RRID: BDSC_64349
Control-spGAL4: BPp65ADZp (attP40); BPZpGDBD (attP2)	Bloomington Stock Center	RRID: BDSC_79603
Wing + haltere CS-spGAL4: R83H05-AD; R31H10-DBD	Bloomington Stock Center	RRID: BDSC_68688; RRID: BDSC_69835
wPN1-spGAL4-1: R53A06-AD; R42D02-DBD	Bloomington Stock Center	RRID: BDSC_ 71089; RRID: BDSC_69077
wPN1-spGAL4-2: R53A06-AD; R50B07-DBD	Bloomington Stock Center	RRID: BDSC_ 71089; RRID: BDSC_69589
Gad1-AD	Bloomington Stock Center	RRID: BDSC_60322
ChAT-DBD	Bloomington Stock Center	RRID: BDSC_60318
Control-GAL4: pBDPGal4U	Bloomington Stock Center	RRID: BDSC_68384
Bristle-GAL4: R38B08-GAL4	Bloomington Stock Center	RRID: BDSC_49541
Control-LexA: pBDPLexAp65U	Bloomington Stock Center	RRID: BDSC_77691
Bristle-LexA: R38B08-LexA	(Jenett et al., 2012)	N/A
R42D02-LexA	Bloomington Stock Center	RRID: BDSC_77691
ChAT-LexA	Bloomington Stock Center	RRID: BDSC_84379
Gad1-LexA	Bloomington Stock Center	RRID: BDSC_60324
VGlut-LexA	Bloomington Stock Center	RRID: BDSC_84442
ChAT-GAL80	Bloomington Stock Center	RRID: BDSC_60321
VGlut-FLP	Bloomington Stock Center	RRID: BDSC_84708
20XUAS-CsChrimson-mVenus (attp18)	Bloomington Stock Center	RRID: BDSC_55134
13XLexAop2-CsChrimson-mVenus (attp18)	Bloomington Stock Center	RRID: BDSC_55137
20XUAS-FRT>STOP>FRT-CsChrimson-mVenus (attP2)	(Shirangi et al., 2016)	N/A
UAS-GtACR2 (attP2)	(Mohammad et al., 2017)	N/A
10XUAS-IVS-eGFPKir2.1 (attP2)	(von Reyn et al., 2014)	N/A
10XUAS-IVS-mCD8::GFP (attP2)	Bloomington Stock Center	RRID: BDSC_32185

(*Continued on next page*)

Continued

REAGENT or RESOURCE	SOURCE	IDENTIFIER
lexAop-rCD2::RFP-p10.UAS-mCD8::GFP-p10 (su(Hw)attP5)	Bloomington Stock Center	RRID: BDSC_67093
10XUAS-IVS-mCD8::RFP (attP18) 13XLexAop2-mCD8::GFP (su(Hw)attP8)	Bloomington Stock Center	RRID: BDSC_32229
UAS-myrGFP.QUAS-mtdTomato-3xHA (su(Hw)attP8); trans-Tango (attP40)	Bloomington Stock Center	RRID: BDSC_77124
UAS-DenMark, UAS-syt.eGFP	Bloomington Stock Center	RRID: BDSC_33065
UAS-CD4-spGFP1-10, lexAop-CD4-spGFP11	(Gordon and Scott, 2009)	N/A
UAS-nSyb-spGFP1-10, lexAop-CD4-spGFP11/ CyO	Bloomington Stock Center	RRID: BDSC_64314
lexAop-nSyb-spGFP1-10, UAS-CD4-spGFP11	Bloomington Stock Center	RRID: BDSC_64315
R57C10-FLP2::PEST	(Nern et al., 2015)	N/A
Software and Algorithms		
MATLAB	http://www.mathworks.com/products/matlab/	RRID:SCR_001622
Python	http://www.python.org/	RRID:SCR_008394
Fiji	http://fiji.sc/	RRID:SCR_002285
VCode	http://social.cs.uiuc.edu/projects/vcode.html	N/A
Automatic Behavior Recognition System (ABRS)	(Ravbar et al., 2019)	https://github.com/AutomaticBehaviorRecognitionSystem/ABRS

RESOURCE AVAILABILITY

Lead contact

Further information and requests for resources should be directed to and will be fulfilled by the Lead Contact, Julie H. Simpson (jhsimpson@ucsb.edu).

Materials availability

All reagents used in this study will be made available on request to the Lead Contact.

Data and code availability

- Ethogram data and one example video are deposited to Mendeley Data with https://doi.org/10.17632/87ngcrv7xw.1
- ABRS code is available on GitHub (https://github.com/AutomaticBehaviorRecognitionSystem/ABRS).
- Any additional information is available from the lead contact upon request.

EXPERIMENTAL MODEL AND SUBJECT DETAILS

Drosophila melanogaster were raised in 25°C incubators with a 12 hr light/dark cycle. For optogenetic experiments, larvae were raised on common corn meal food. After eclosion, one-day old adults were transferred into food containing 0.4 mM all-*trans*-retinal. We then raised the files in dark for another 2–3 days before experiments.

METHOD DETAILS

Immunofluorescence and confocal imaging

For central nervous system (CNS) immunostaining, whole flies immobilized with an insect pin through the abdomen were fixed in 4% PFA for 2 hours on a nutator at room temperature. After three 1 min wash in PBT, flies were dissected in the PBS buffer to get the whole CNS. CNS samples were further washed three times in 1 min PBT and then blocked for 30 min in 4% NGS. Staining with primary antibody was performed in 4°C overnight on a nutator. Samples were then washed 3 times for 20 min in PBT. Secondary antibody incubation was performed for 2 hours at room temperature. Samples were washed again in PBT for 3 times and

mounted in VectaShield for imaging. To check GFP expression in the wing sensory neurons, whole flies were washed in 100% ethanol and then PBS; wings were then pulled and mounted in VectaShield on a microscope slide for imaging. The following primary antibodies were used: rabbit polyclonal to GFP (Invitrogen A-11122, 1:1000), chicken polyclonal to GFP (Abcam 13970, 1:1000), rabbit anti-HA (Cell Signaling Technologies C29F4, 1:300) and mouse monoclonal Brp antibody (DSHB nc82, 1:300). All secondary antibodies were diluted at 1:500. Confocal images were taken on a Zeiss LSM710 microscope. Images were then processed in ImageJ.

In *trans*-Tango experiments, 14–20 days adult flies raised at 18°C were used. In GRASP experiments, adult flies were raised at 25°C for 14–20 days before dissection. Mouse anti-GFP antibody (Sigma-Aldrich G6539, 1:100) was used to detect the reconstructed GFP in GRASP experiments.

Optogenetic activation experiments of free-moving flies

After cold anesthesia, flies were left to recover in the recording chamber for at least 20 min. Custom-made LED panels (LXM2-PD01-0050, 625 nm) were used for light activation from below. 20 Hz 20% light duty cycle was used in all experiments. LED power was adjusted according to the expression level and behavioral response of different lines. Light intensity was measured by a Thorlabs S130VC power sensor coupled with a PM100D console. The light intensity used in the experiments are: *Control-spGAL4* (8.4 mW/cm^2), *Wing haltere CS-spGAL4* (5.6 mW/cm^2), *wPN1-spGAL4-1* (2.8 mW/cm^2), *wPN1-spGAL4-2* (1.4 mW/cm^2), *Control-GAL4* (8.4 mW/cm^2), *R42D02-GAL4* (1.4 mW/cm^2), *Control-LexA* (11.2 mW/cm^2), *R42D02-LexA* (11.2 mW/cm^2). 30Hz videos were recorded by an IDS UI-3370CP-C-HQ camera and manually annotated in VCode or automatically annotated by ABRS (https://github.com/AutomaticBehaviorRecognitionSystem/ABRS). For high-resolution example videos in Figure 1D, a 10mm diameter quartz chamber was used, and videos were recorded from below. A FLDR-i132LA3 red ring light (626 nm) was used for optogenetics activation.

Recording and analysis of dust-induced grooming with optogenetic inhibition

Grooming behavior in response to dust was assayed as described previously (Seeds et al., 2014; Zhang et al., 2020). In short, flies were put into the 4 middle wells of 24-well corning tissue culture plate with 5 mg dust and shaken for 10 times. 30 Hz videos were recorded for 22 min with a FLIR Blackfly S BFS-U3-13Y3M-C camera. Infrared backlight was used for illumination. Custom-made LED panels (TT Electronics OVSPRGBCR4, 465nm) were used for light inhibition. Constant 2.1 mW/cm^2 blue light was delivered from below in all experiments. Videos were processed through ABRS to generate ethograms. For dust visualization in Figure 2A, flies were quickly transferred to another recording setup with white light illumination. Grooming modules were described previously (Seeds et al., 2014).

Fly-on-a-ball experiment

The experimental rig was described previously (Seelig et al., 2010) with modifications. In short, a decapitated 3-day female was tethered to a size 1 insect pin through UV glue. Air flow (500–600 mL/min) passed through water for humidification was used to support the 10mm diameter foam ball (LAST-A-FOAM FR-7120 material). A 10μL extended length pipette tip attached to a micromanipulator was used to deliver ~2Hz mechanosensory stimuli to the posterior wing edges. A Doric Lenses fiber LED (CLED_469) with custom-made collimator was used to target the light to the thorax. 44μW constant blue light was used in all experiments (Light power rather than intensity was used since it is hard to measure illumination area). 100Hz videos were recorded with a FLIR Blackfly S BFS-U3-13Y3M-C camera and manually annotated in VCode. The experimenter was blind to the fly genotype.

QUANTIFICATION AND STATISTICAL ANALYSIS

Data analysis was performed in MATLAB 2017b. Wilcoxon signed-rank test was used for two related samples. Wilcoxon rank-sum test was used for two independent samples. Kruskal-Wallis test and Wilcoxon rank-sum post hoc with Bonferroni correction were used for three or more independent samples.

Data was plotted with notBoxPlot (https://github.com/raacampbell/notBoxPlot) function. Each dot is one fly. The mean is shown as a blue line, 95% confidence intervals for the mean are shown as dark shades. The median is shown as a dotted red line. One standard deviation is shown as light color shade. *$p < 0.05$; **$p < 0.01$; ***$p < 0.001$.